

Polyakov loop in 2+1 flavor QCD

A. Bazavov¹ and P. Petreczky¹

¹ *Physics Department, Brookhaven National Laboratory, Upton, NY 11973, USA*

We study the temperature dependence of the renormalized Polyakov loop in 2+1 flavor QCD for temperatures $T < 210$ MeV. We extend previous calculations by the HotQCD collaboration using the highly improved staggered quark action and perform a continuum extrapolation of the renormalized Polyakov loop. We compare the lattice results with the prediction of non-interacting static-light hadron resonance gas, which describes the temperature dependence of the renormalized Polyakov loop up to $T < 140$ MeV but fails above that temperature. Furthermore, we discuss the temperature dependence of the light and strange quark condensates.

PACS numbers:

I. INTRODUCTION

At high temperature strongly interacting matter undergoes a transition to a new state characterized by deconfinement and color screening (see e.g. Refs. [1, 2] for recent reviews). The Polyakov loop is an order parameter for deconfinement phase transition in $SU(N)$ gauge theories. After proper renormalization it is related to the free energy of a static quark F_Q [3, 4]. More precisely, it can be defined through the difference in the free energy of a system containing a static quark anti-quark ($Q\bar{Q}$) pair at infinite separation and a system without static charges at the same temperature $F_\infty(T)$, i.e. $L_{ren}(T) = \exp(-F_\infty(T)/2T) = \exp(-F_Q/T)$ [3]. In the confined phase $F_\infty = \infty$ since the static Q and \bar{Q} cannot be separated to infinite distance. Consequently, the Polyakov loop which transforms non-trivially under the center of the gauge group is zero. In the deconfined phase the static quark and anti-quark could be separated to infinite distance due to color screening which means breaking of the center symmetry $Z(N)$ [5, 6]. Dynamical quarks explicitly break the $Z(N)$ symmetry of the partition function and F_∞ is finite since the static Q and \bar{Q} can be now separated to infinite distance by creating a dynamical quark anti-quark pair from the vacuum, a phenomenon often called string breaking. In 2+1 flavor QCD with the quark masses realized in nature there is no phase transition related to deconfinement. Moreover, the renormalized Polyakov loop cannot be related to the singular part of the free energy density [7, 8]. However, the renormalized Polyakov loop is sensitive to the color screening in hot QCD medium, at high temperature it is closely related to the Debye screening mass (see e.g. [9]). In the opposite limit of very low temperatures F_Q is related to the binding energy of a static-light meson (see e.g. [10]). Thus, the renormalized Polyakov loop is a good probe of the hot strongly interacting medium.

On the lattice with temporal extent N_τ the renormalized Polyakov loop is calculated according to the following formula:

$$L_{ren}(T) = \exp(-cN_\tau/2) \left\langle \frac{1}{3} \text{Tr} \prod_{x_0=1}^{N_\tau} U_0(x_0, \vec{x}) \right\rangle, \quad (1)$$

where $U_0(x_0, \vec{x})$ is the gauge link variable in the time direction and c is the lattice spacing dependent normalization constant that ensures that the static potential calculated on the lattice has a certain value at a chosen distance [11]. In the recent past the renormalized Polyakov loop has been calculated on the lattice in 2+1 flavor QCD with physical quark masses using the improved staggered fermion formulation [7, 8, 11–14]. Furthermore, using the stout improved staggered action continuum results for the renormalized Polyakov loop have been presented [14]. The aim of this paper is to study the renormalized Polyakov loop in the low temperature and transition regions and to perform an independent continuum extrapolation using the highly improved staggered quark (HISQ) action [15]. While the temperature dependence of the Polyakov loop in QCD at high temperatures is very similar to its temperature dependence in pure gauge theory, this is not the case for the low temperature and the transition regions. To understand at which temperature color screening effects set in, it is important to clarify to what extent the temperature dependence of the Polyakov loop can be understood in terms of hadrons. As mentioned above, at very low temperatures the dominant contribution to F_Q is given by the lowest static-light state. As the temperature increases, more massive states will contribute as well and also the interactions of static-light hadrons with the medium will become more important. For the description of the bulk thermodynamic quantities it turns out that interactions between hadrons can be taken into account by adding the contribution of hadronic resonances. It is reasonable to assume that the effects of interactions of static-light hadrons with the hadrons in the medium can be accounted for by adding excited (resonance) states. Therefore, we calculate the renormalized Polyakov loop in the approximation of non-interacting gas of static-light hadrons and hadronic resonances as has been suggested recently [16]. Contrary to Ref. [16] (see also [17, 18]), where the experimental spectrum of heavy-light(strange) hadrons was used together with different model considerations, our analysis is largely based on the lattice QCD calculations of the spectrum of static-light and static-strange hadrons [19, 20]. We also consider different quark model analyses of the heavy-light(strange) hadron spectrum, compare them with each other and the

available lattice calculations, and use them to estimate the contribution of higher lying excited states to L_{ren} .

The rest of the paper is organized as follows. In section II we present our numerical results for the renormalized Polyakov loop. The temperature dependence of the quark condensates is also discussed there. In section III we discuss the spectrum of static-light hadrons and the calculation of the Polyakov loop using the hadron resonance gas approximation for static-light hadrons. Finally, section IV contains our conclusions.

II. NUMERICAL RESULTS

The chiral and deconfining aspects of the QCD transition have been studied by the HotQCD collaboration using lattices with temporal extent $N_\tau = 6, 8, \text{ and } 12$ and a combination of the tree-level improved gauge action and the HISQ action in the quark sector [8]. This combination of the gauge action and quark action was referred to as the HISQ/tree action in Ref. [8] but here we refer to it as the HISQ action for simplicity. For reliable continuum extrapolations we need at least three lattice spacings. Therefore, we performed calculations using $40^3 \times 10$ lattices, using as in the earlier work the rational hybrid Monte-Carlo algorithm [21]. The algorithmic details of dynamical HISQ simulations can be found in Ref. [22]. As in Ref. [8], calculations are performed for the physical value of the strange quark mass m_s and light quark masses $m_l = m_s/20$. This light quark mass corresponds to the pion mass of 160 MeV in the continuum limit [8], which is slightly above the physical value. However, for the Polyakov loop this small difference from the physical value plays no role. The parameters of the lattice simulations including the lattice gauge coupling $\beta = 10/g^2$ and the strange quark mass in lattice units are shown in Table I along with the corresponding temperatures. The last column of the table shows the accumulated statistics for each β value in terms of molecular dynamics time units. The lattice spacing a is determined from the r_1 parameter defined in terms of the zero-temperature static potential as

$$r^2 \frac{dV}{dr} \Big|_{r=r_1} = 1.0, \quad (2)$$

and we use the value $r_1 = 0.3106 \text{ fm}$ [23]. We use the parametrization of the lattice spacing and the quark masses as functions of the gauge coupling β along the lines of constant physics that are given in Ref. [8]. The β dependent normalization constant c that enters Eq. (1) was also taken from Ref. [8]. Since we are interested in the low temperature behavior of the Polyakov loop, we also performed additional calculations on $32^3 \times 8$ lattices for three values of the temperature, $T = 116 \text{ MeV}, 125 \text{ MeV}$ and 131 MeV . The corresponding simulation parameters are also given in Table I. Our calculations extend to temperatures as low as 116 MeV, which is lower than in any previous lattice study. Our numerical results

for the Polyakov loop are shown in Fig. 1. To obtain continuum results for the renormalized Polyakov loop we first perform a smooth spline interpolation of the numerical data for each N_τ . The errors of the spline interpolation are determined using the bootstrap method. Then we perform continuum extrapolations at selected temperature values from $T = 120 \text{ MeV}$ to 210 separated by 5 MeV steps. In addition we also consider the renormalized Polyakov loop at $T = 117 \text{ MeV}$. Since the leading discretization errors in the staggered fermion formulation are proportional to a^2 , we expect that for the renormalized Polyakov loop they should scale like $(aT)^2 = 1/N_\tau^2$. Therefore we performed $1/N_\tau^2$ extrapolation of the renormalized Polyakov loop for $T \geq 135 \text{ MeV}$, where we have at least three lattice spacings. At lower temperatures we have only two lattice spacings to estimate the continuum limit, corresponding to $N_\tau = 8$ and 10. Furthermore, as one can see from Fig. 1 (right) the lattice data do not show a clear N_τ dependence at these temperatures within the estimated errors. Moreover, the ordering of the $N_\tau = 8$ and $N_\tau = 10$ data seems to be the opposite of that at $T > 135 \text{ MeV}$. For this reason we estimate the continuum limit for L_{ren} at $T \leq 135 \text{ MeV}$ by averaging the interpolated $N_\tau = 8$ and $N_\tau = 10$ data.

Our continuum estimates for the renormalized Polyakov loop are also shown in Fig. 1 and are compared with the continuum results obtained using the stout action [14]. The two lattice extrapolated continuum results agree with each other, except for $T = 140 \text{ MeV}$, where our results are larger by two standard deviations.

As discussed in section I the deconfinement phase transition is related to $Z(N)$ symmetry in the case of infinitely heavy quarks. In the opposite limit of massless quarks there is a chiral restoring phase transition. The connection between the deconfinement crossover and the chiral crossover in QCD with the physical values of the quark masses is a subject of long-standing discussions (see e.g. Refs. [24–26]). Therefore, it is interesting to compare the temperature dependence of the renormalized Polyakov loop in the continuum limit to the temperature dependence of the chiral condensate which is used to describe the chiral aspects of the QCD crossover. Combining our numerical results with the published HotQCD [8] results we estimated the renormalized chiral condensates Δ_{ls} and Δ_l^R defined in Ref. [8] in the continuum limit. So far continuum extrapolated data for the chiral condensate are only available for the stout action. The details of this analysis are given in the Appendix, where we also compare our results with the one obtained using the stout action. We also calculated the strange quark condensate Δ_s^R , which is analogous to Δ_l^R (see Ref. [8]) in the continuum limit. The details of these calculations are also given in the Appendix.

In Fig. 2 the temperature dependence of the Polyakov loop is compared with the temperature dependence of the renormalized chiral condensate as well as with the temperature dependence of the strange quark condensate. As one can see from the figure the renormalized

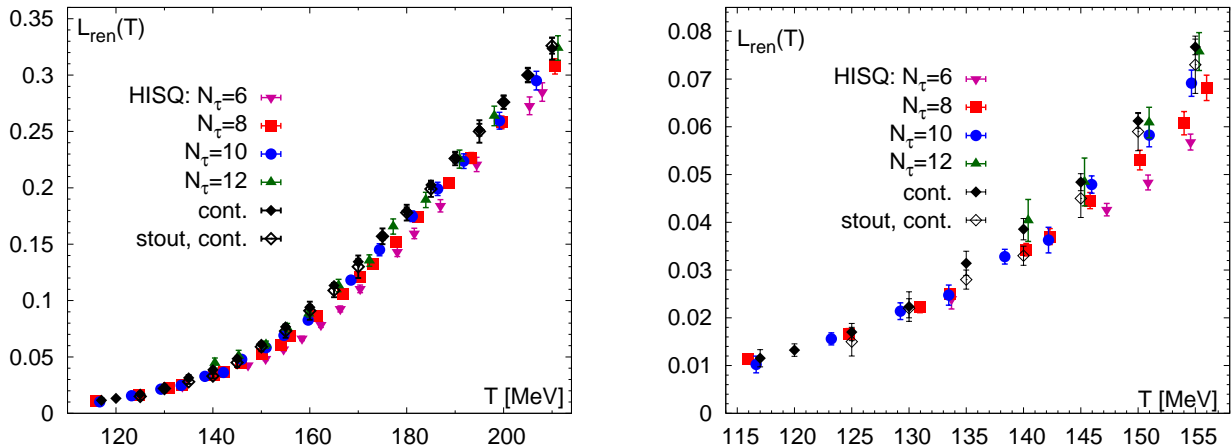


FIG. 1: The renormalized Polyakov loop calculated with the HISQ and stout action. The HISQ results for $N_\tau = 6, 8$ and 12 are from Ref. [8]. The continuum stout data are from Ref. [14]. The filled diamonds correspond to the continuum extrapolation for the HISQ action. The right panel shows the closeup of the Polyakov loop in the low temperature region.

β	m_s	T [MeV]	$\#TU$
$N_\tau = 10$			
6.285	0.0790	117	2423
6.341	0.0740	123	7679
6.390	0.0694	129	4990
6.423	0.0670	133	3640
6.460	0.0642	138	4200
6.488	0.0620	142	3370
6.515	0.0604	146	4988
6.550	0.0582	151	4990
6.575	0.0564	155	4990
6.608	0.0542	160	4990
6.664	0.0514	168	5000
6.700	0.0496	174	4990
6.740	0.0476	181	4990
6.770	0.0460	186	4990
6.800	0.0448	192	5310
6.840	0.0430	199	4990
6.880	0.0412	207	4990
$N_\tau = 8$			
6.050	0.1064	116	3977
6.125	0.0966	125	3180
6.175	0.0906	131	3732

TABLE I: Simulation parameters for $40^3 \times 10$ and $32^3 \times 8$ lattices. The last column shows the accumulated statistics in terms of molecular dynamics trajectories.

Polyakov loop changes very smoothly in the temperature interval where the chiral condensates drops rapidly and it is difficult to tell whether the transition in the renormalized Polyakov loop and chiral condensates are connected. Comparison with the hadron gas model described in the

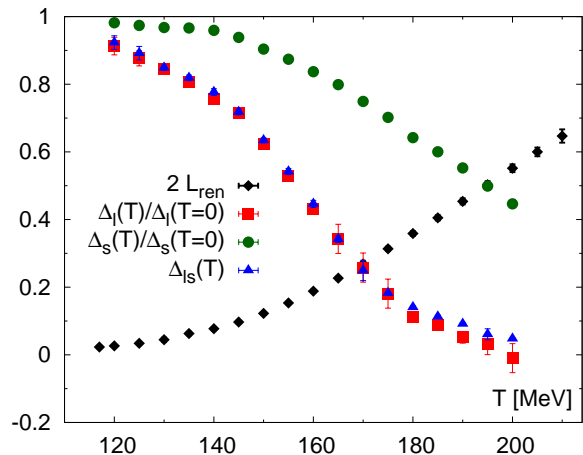


FIG. 2: The temperature dependence of the renormalized Polyakov loop compared to the temperature dependence of the renormalized chiral condensates Δ_I^R and Δ_{Is} as well as the strange quark condensate Δ_s^R . The values of Δ_I^R and Δ_s^R have been normalized by the corresponding zero temperature values. Δ_{Is} goes to one in the zero temperature limit by construction. All results are continuum extrapolated.

next section, however, can provide further insight into this issue. Finally, the strange quark condensate shows a smooth behavior similar to that of L_{ren} .

III. THE HADRON GAS MODEL

As discussed in section I, at very low temperature the free energy of a static quark is largely determined by the binding energy of the lowest static-light meson. In addition, there are contributions from static-strange mesons and baryons with one static quark. Thus, following Ref.

[16], at very low temperature the Polyakov loop is given by the contribution of the lowest static-light states

$$3L_{ren} = 4 \exp(-M/T) + 2 \exp(-M_s^0/T) + \sum_I \sum_j (2I+1)(2j+1) \exp(-M_{I,j}^{B0}/T), \quad (3)$$

where the spin and iso-spin degeneracies of the meson states have been taken into account and the summation of all iso-spin (I) states, as well as of all light and/or strange quark angular momentum states (j) for the lowest static-light baryons. Altogether we have contributions from 6 mesons and 21 baryons [16]. The factor 3 on the left-hand side of the above equation originates from the color normalization in the definition of L_{ren} in Eq. (1) and can be seen from the spectral decomposition of the Polyakov loop correlator derived in [27]. Interactions with the medium are suppressed at very low temperatures but start to become more important as the temperature increases. One may try to include the interaction by assuming that it can be approximated by resonances. This assumption seems to work quite well for bulk thermodynamic quantities [14, 28–30]. The static-light meson contains a divergent self-energy contribution which needs to be subtracted. This leaves the mass of the ground static meson state undetermined, while the masses of all other states are given with respect to the mass of the lightest state $E_i = M_i - M_0$. Therefore, we can generalize the above equation as follows:

$$L_{ren} = \frac{1}{3} \exp(-\Delta/T) (4 + 2 \exp(-E_0^s/T) + \sum_{n,I,j} (2I+1)(2j+1) \exp(-E_{n,I,j}/T)). \quad (4)$$

Here E_0^s is the energy of the lightest static-strange meson with respect to the mass of the lowest static-light state M_0 . The first and the second terms correspond to the contribution of the ground state static-light and static-strange mesons, while the third term corresponds to the contribution of the baryon states and the excited meson states. The index n denotes different excited states corresponding to the same values of I and j . The renormalized Polyakov loop depends on the subtracted mass of the lowest static-light meson Δ . This needs to be adjusted to match the lattice data for the Polyakov loop at low temperatures, i.e. Δ should be adjusted to the specific scheme used for the normalization of the Polyakov loop on the lattice. This matching procedure will be discussed in subsection C. In the following two subsections we are going to discuss the meson and baryon contributions to L_{ren} separately.

A. Static mesons and their contribution to the renormalized Polyakov loop

Static-light and static-strange mesons are characterized by the angular momentum of the light (strange) quark and parity j^P . The spectrum of static-light mesons consists of approximately degenerate pairs with

$j = |l \pm 1/2|$, where l is the orbital angular momentum. The spectrum of static-light(strange) mesons has been studied in 2-flavor lattice QCD by the ETMC collaboration for j up to 7/2 that correspond to orbital angular momentum $l = 0, 1, 2$ and 3 and are denoted by S , P_\pm , D_\pm , F_\pm [19]. Also the masses of first static-light and static-strange excited meson states for $1/2^-$ channel (first radial or S^* state in the ETMC notation) have been calculated [19]. To get rid of the divergent self-energy contribution, the masses of different states are calculated with respect to the ground state (S state) mass both in the light and the strange quark sectors. These mass differences have been extrapolated to the continuum limit and to the physical pion mass and are approximately the same for static-light and static-strange mesons, see Table 5 of Ref. [19]. The errors for the above mass difference vary between 12 MeV and 37 MeV. With all the spin and iso-spin degeneracies the number of states identified on the lattice is 96. To calculate the Polyakov loop according to Eq. (4) we need to know E_0^s , the energy (mass) of the lowest static-strange meson with respect to the lightest static-light meson. We use phenomenological considerations to do so. Consider the spin-averaged mass of the ground state charmed (bottom) mesons with strangeness $S = 0$ and $S = -1$:

$$\overline{M}_D = \frac{3M(D^*) + M(D)}{4} = 1975 \text{ MeV}, \quad (5)$$

$$\overline{M}_B = \frac{3M(B^*) + M(B)}{4} = 5314 \text{ MeV}, \quad (6)$$

$$\overline{M}_{D_s} = \frac{3M(D_s^*) + M(D_s)}{4} = 2076 \text{ MeV}, \quad (7)$$

$$\overline{M}_{B_s} = \frac{3M(B_s^*) + M(B_s)}{4} = 5404 \text{ MeV}. \quad (8)$$

Here we used the values of the charm and bottom meson masses from Particle Data Group [31]. We get $\overline{M}_{D_s} - \overline{M}_D = 100$ MeV and $\overline{M}_{B_s} - \overline{M}_B = 90$ MeV. Heavy quark effective theory predicts that the masses of heavy-light mesons and thus also the above difference should scale as the inverse of the heavy quark mass m_Q . Using this and the values of \overline{M}_D and \overline{M}_B as proxies for the charm and bottom quarks respectively we get a value of 84 MeV for the difference of the lowest static-strange and static-light meson mass, i.e. $E_0^s = 84$ MeV for $m_Q = \infty$. It is interesting to mention that the value of the strange quark mass in the \overline{MS} scheme, $m_s(\mu = 2 \text{ GeV}) = 95(5)$ MeV, is close to the value of E_0^s . So E_0^s may be interpreted as a constituent strange quark mass.

To study the contribution of higher excited states we will use the D_s meson spectrum calculated on the lattice [32] as well as in a relativistic quark model [33–36]. The spectrum of D_s mesons has been calculated on the lattice using improved Wilson fermion actions [32]. One needs to establish a relation between the meson masses in the static case and the masses of D_s mesons. Heavy mesons, D_s mesons in particular, are characterized by nL_J , with J being the total angular momentum of the meson, L being the orbital momentum and n being the

radial quantum number. Obviously the $j = 0$ states in the static limit are identified with spin-averaged S -state D_s mesons. For a finite heavy quark mass, the $L - 1/2$ state in the static limit splits into two states, L_{L-1} and L_L , while the $L + 1/2$ state splits into L_L and L_{L+1} state, e.g., P_- becomes $1P_0$ and $1P_1$, and P_+ becomes $1P_1$ and $1P_2$. The corresponding splittings, however, are small. Such a degeneracy pattern is indeed observed in the experimentally established positive parity (P -wave) D and D_s mesons. Furthermore, the mass differences of various D_s meson states calculated on the lattice and the spin-averaged lowest S -state are in reasonable agreement with the mass differences in the static limit discussed above. Therefore, it is justified to use the D_s meson masses calculated on the lattice as proxies for static-strange mesons. Since the above difference is approximately the same for strange and light quark cases we can use the same mass difference also for the light quarks. That allows us to include the following excited states into the analysis: $2P$, $2D$, and $2F$. We identify the mass of $2L_-$ meson in the static case with the lowest $2L_L$ D_s meson mass and the $2L_+$ with the higher $2L_L$ D_s meson. With all the spin-iso-spin degeneracies this gives 90 states.

To include even higher excited states we use quark model predictions. The quark model can predict certain qualitative features of the heavy-light and static-light meson spectrums correctly [33–35]. However, the quark models also have problems. In the static limit the mass of the P_+ state is smaller than the mass of the P_- state just the opposite of what is observed on the lattice [19]. The mass of the P_+ in a quark model, calculated in Ref. [35], is 230 MeV below the lattice result. Similarly, the mass of the $2S$ state is 441 MeV below the lattice result [19]. Comparing the results of Refs. [33, 34] to Ref. [35], one may conclude that the model dependence is small for the $1P$ meson states, however, in the B_s sector the masses of the $2S$ states differ by about 300 MeV. We try to account for these problems by assigning a theoretical error to the masses of higher excited states.

We took the results of quark model calculations of D and D_s mesons [36] to estimate the contribution of $3S$, $4S$, $5S$, $3P$, and $1G$ states. From comparison of the results of different quark models, as well as the comparison to the lattice results discussed above, we estimate the uncertainty of the masses of the higher nS states ($n \geq 3$) to be 300 MeV, while for the other states we estimate it to be 150 MeV. It turns out, however, that contribution of these states to L_{ren} is negligible up to temperatures of 210 MeV for which the model makes sense. The excited states discussed so far should include all the possible states up to masses of 2 GeV above the ground state mass. It is unlikely that individual resonance states can be observed above that energy. In Fig. 3 we show the contribution of meson states to the renormalized Polyakov loop. We normalize the results by $L_0 = 4 \exp(-\Delta/T)/3$. The contribution of all static meson states calculated on the lattice in Ref. [19] is shown as the band, the dashed line includes the con-

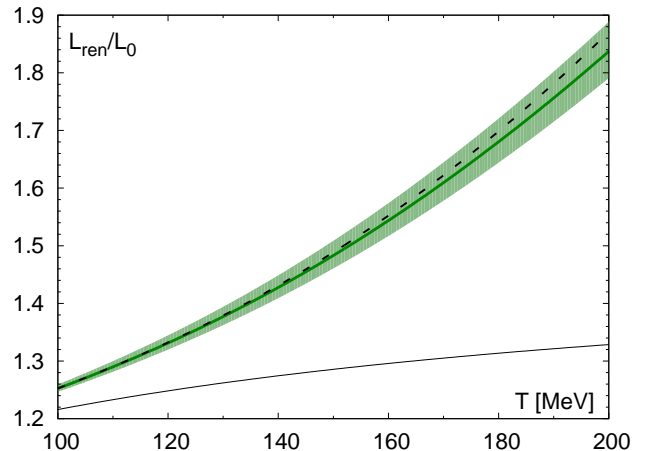


FIG. 3: Meson contribution to L_{ren} normalized by $L_0 = 4 \exp(-\Delta/T)/3$. The band shows the contribution of all static meson states calculated on the lattice (see text). The dashed line includes the contribution of higher excited states. The thin solid line corresponds to the contribution of the lightest static-strange meson only.

tribution of the higher excited states, and the thin solid line corresponds to the first static-strange meson only. The uncertainty band is determined by the errors of the static meson masses calculated on the lattice [19]. We see that at low temperatures the only meson state that has a significant contribution to L_{ren} in addition to the lowest state is the lightest static-strange meson, though the contribution of excited states cannot be completely neglected. Excited states (up to $1F$) become very important at higher temperatures, $T > 140$ MeV. Finally, the contribution of higher excited states is quite small and is only visible for $T > 170$ MeV.

B. Baryon contribution to the renormalized Polyakov loop

The spectrum of baryons with one static quark has been studied by the ETMC collaboration [20] in 2 flavor QCD. The masses of static baryons with positive and negative parity and angular momentum of light quarks $j = 0$ and 1 have been calculated. These states correspond to the ground state and first orbital excitation of baryons with one heavy quark, i.e., to $1/2^+$, $3/2^+$ and $1/2^-$ and $3/2^-$. Counting the iso-spin and angular momentum degeneracies, the lowest positive and negative parity baryons correspond to 79 states. The calculations have been carried out at one lattice spacing. The lack of continuum extrapolation is not of great concern, since based on the studies of the static meson spectrum, cutoff effects are expected to be small compared to the statistical errors. The results presented in Ref. [20] depend somewhat on how the lattice spacing is set. More precisely, using f_π the lattice spacing was determined to

be $0.079(3)$ fm, while using the nucleon mass the lattice spacing turned out to be $0.089(5)$ fm. In our analysis we use the values of the masses obtained by fixing the lattice spacing through the nucleon mass m_N , since this procedure gives a value of the r_0 parameter that is consistent with other determinations [8, 13], namely $r_0 = 0.473 \pm 0.09(\text{stat.}) \pm 0.16(\text{syst.})$ fm [37]. Setting the scale with f_π gives $r_0 = 0.42$ fm [38] which is much smaller than any other determination. The lowest lying positive and negative parity baryons give a fairly large contribution to the renormalized Polyakov loop, in fact, the largest contribution next to the ground state mesons. However, it turns out that higher excited states cannot be neglected. We can use quark models to estimate the contribution of higher lying baryon states to L_{ren} .

The spectrum of baryons containing one heavy (c or b) quark has been studied in the relativistic quark model [39] and in the relativistic quark-diquark model [40]. The analysis of Ref. [39], however, was restricted to $\Lambda_{b,c}$ and $\Sigma_{b,c}$ baryons. We will use the spectrum of excited heavy baryons containing a b quark as a proxy for the spectrum of higher excited baryon states with a static quark. The masses of baryons with a static quark are determined by the angular momentum of the light quarks j . Therefore, the heavy baryons form doublets with almost the same mass that correspond to the same angular momentum j of the light quarks and total angular momentum $J = j \pm 1/2$. In our analysis we consider the mass difference of the baryon with the lower angular momentum in the doublet and the spin averaged mass of $B(B^*)$ mesons. These mass differences obtained in a quark model are compared to the static baryon spectrum for the lowest positive and negative parity states calculated on the lattice. It turns out that the agreement between the lattice results and the model calculations is quite good if the nucleon mass is used to set the lattice spacing. In fact, the lattice results agree with the model calculations within the errors. For the Λ_b and Σ_b families we also find good agreement between the diquark model and Ref. [39] for the lowest states of both parities. In our calculations we use the spectrum calculated in Ref. [40] which corresponds to baryon states with angular momenta up to $J = 11/2$ equivalently to $j = 5$ of the light quarks and up to 5 radial excitations. Counting all the spin and iso-spin degeneracies these correspond to 984 states.

As discussed above, different model calculations agree with each other for the lowest positive and negative parity states. Unfortunately, the agreement is not that good for the higher excited states. To estimate the sensitivity of the Polyakov loop to the model uncertainty of the higher excited baryon states we calculated the contribution of excited Λ_Q and Σ_Q baryons to L_{ren} , including all states up to $J = 7/2$, using the results of Ref. [39] and of the diquark model [40]. The contributions of Λ_b to L_{ren} are a factor of two larger if one uses the spectrum from Ref. [39] compared to the case where the Λ_b spectrum from the diquark model is used. On the other hand, the contribution of the Σ_b baryons is a factor of two smaller

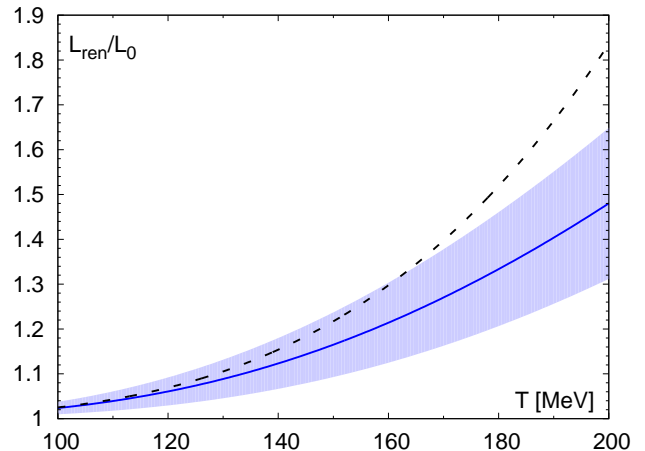


FIG. 4: The contribution of baryons to L_{ren} normalized by $L_0 = 4 \exp(-\Delta/T)/3$. The solid line and the band correspond to the contribution of the lowest positive and negative parity baryons, while the dashed line corresponds to the contribution of all baryon states.

if one uses the results of Ref. [39] instead of the results of the diquark model. Therefore we estimate that contribution of the higher excited baryon states is uncertain by a factor 2.5. This is the largest source of uncertainty in the hadron resonance gas model for $T > 170$ MeV. The contribution of baryons to the renormalized Polyakov loop is shown in Fig. 4. The contribution of the static baryons identified on the lattice in Ref. [20] is shown as the solid line and the band. The error band corresponds to the uncertainty that has been evaluated using the errors on the static baryon masses. The contribution of all baryon states to L_{ren} is shown as the dashed black line. At temperatures $T < 120$ MeV the contribution of the baryons is below 10%. It becomes significant above that temperature. The contribution of higher excited states becomes significant only for $T > 140$ MeV. Therefore, as will become clear in the next subsection, the uncertainty in the comparison to the lattice data due to the excited states is small.

C. Comparison with lattice results

Let us compare the hadron resonance gas model results with the lattice data discussed in section II. The comparison is easiest in terms of the free energy of an isolated static quark $F_Q(T) = -T \ln L_{ren}(T)$. The renormalization procedure of the Polyakov loop on the lattice introduces a scheme dependence. Therefore, for the comparison of the hadron resonance gas with the lattice data one needs to adjust the parameter Δ in Eq. (4). We fix Δ by requiring that the hadron resonance gas model matches the continuum lattice result at the lowest temperature $T = 117$ MeV. This gives $\Delta = 593 \pm 18$ MeV. Once this constant is fixed, the hadron resonance gas model can

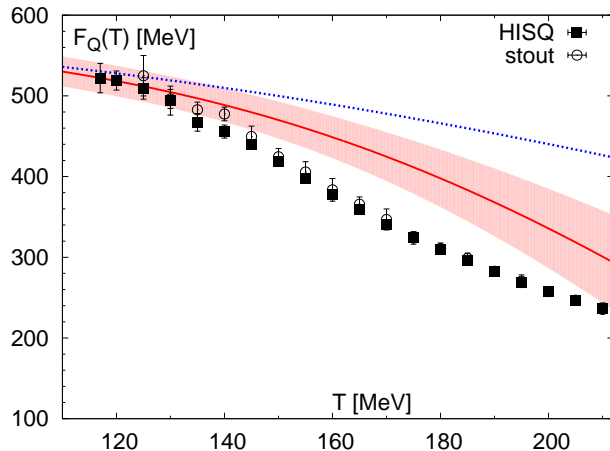


FIG. 5: The free energy of a static quark $F_Q(T)$ calculated on the lattice and compared with the resonance gas model (solid line). The uncertainty of the hadron resonance gas model is indicated by the band. The dotted line is the hadron resonance gas model result with the ground state meson and baryon contribution only.

predict the free energy of an isolated static quark at any other temperature.

The comparison of the lattice data with the hadron resonance gas model is shown in Fig. 5. The solid line and the band correspond to the hadron resonance gas results with all the states discussed above and their uncertainty, which also includes the uncertainty in the value of Δ . The dashed line corresponds to the contribution of the ground states only. The figure shows that the contribution of excited states is significant already for the lowest temperature available in the lattice calculations. The hadron resonance gas model can describe the lattice results on the renormalized Polyakov loop up to temperature 140 MeV, however, clearly fails above that temperature. All the excited states included in the analysis are not sufficient to explain the rapid decrease of the static quark free energy. This result agrees qualitatively with the findings of Ref. [16] if the stout data for $T < 140$ MeV are used to normalize the static free energy in their analysis (cf. Fig. 4 of Ref. [16]). More work is needed to understand the discrepancy between the lattice data and the hadron resonance gas model. It is possible that exotic hadron states can explain the discrepancy between the lattice results and the hadron resonance gas model for $T > 140$ MeV. Another possibility could be the partial restoration of the chiral symmetry and the corresponding change in the static-light hadron masses, as indicated in a recent lattice study [41].

IV. CONCLUSIONS

We studied the renormalized Polyakov loop in lattice QCD using the HISQ action and obtained results

in the continuum limit for temperatures $120 \text{ MeV} < T < 210 \text{ MeV}$. Results obtained with the HISQ action are in the a^2 scaling regime for $N_\tau \geq 6$. Our continuum results agree well with the earlier findings obtained using the stout action [14]. We also revisited the temperature dependence of the quark condensates and find that in the temperature region, where the light quark condensates show a rapid decrease, the renormalized Polyakov loop changes very smoothly. We do not see an obvious connection between the chiral and deconfinement transition described in terms of these quantities.

We studied the question of the physics origin behind the increase in the Polyakov loop, or equivalently, the decrease in the free energy of a static quark F_Q . At sufficiently high temperatures the decrease in F_Q is associated with the onset of color screening which also leads to the same decrease in the energy of a static quark at leading order [42]. For temperatures $T < 140$ MeV the decrease in F_Q could be explained in terms of the hadron resonance gas model. For larger temperatures the decrease in F_Q appears to be significantly larger and cannot be explained in terms of conventional static-light(strange) hadron states. It remains to be seen whether this rapid decrease is due to the contribution from exotic static-light hadrons or some other mechanism. In the latter case its implication for color screening is not clear, especially in view of recent lattice results on the static energy of $Q\bar{Q}$ pair which do not indicate large significant screening effects for $T < 200$ MeV [43, 44]. Currently one of the largest uncertainties in the Polyakov loop calculations within the hadron resonance gas model comes from the excited baryon states. Clearly an improved lattice calculation of the static baryon spectrum would be very helpful in this regard. Another open issue is the contribution of exotic static-light hadron states.

Appendix: Temperature dependence of the quark condensates

In this appendix we discuss the calculation of the renormalized quark condensates. The quark condensate $\langle \bar{\psi}\psi \rangle_q$ needs a multiplicative renormalization, and for non-zero quark masses also an additive renormalization. It is easy to see that the leading additive divergence is proportional to the quark mass and is quadratic in the cutoff (inverse lattice spacing). Therefore, studying the following combination, called the subtracted quark condensate, was proposed [12]:

$$\Delta_{l,s}(T) = \frac{\langle \bar{\psi}\psi \rangle_{l,\tau} - \frac{m_l}{m_s} \langle \bar{\psi}\psi \rangle_{s,\tau}}{\langle \bar{\psi}\psi \rangle_{l,0} - \frac{m_l}{m_s} \langle \bar{\psi}\psi \rangle_{s,0}}. \quad (9)$$

Here $q = l$ and s correspond to light and strange quarks, while the subscripts $x = 0, \tau$ refer to zero and finite temperature expectation values, respectively. The expectation values $\langle \bar{\psi}\psi \rangle_{q,x}$ are normalized per single flavor. Sub-leading divergences proportional to the quark mass cubed

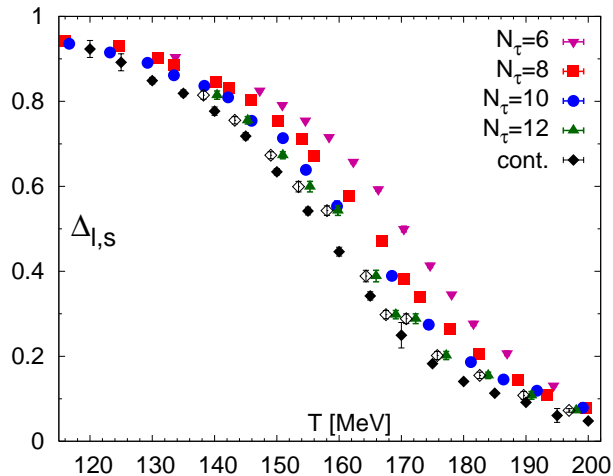


FIG. 6: The subtracted chiral condensate calculated with the HISQ action. The open diamonds correspond to the $N_\tau = 12$ results obtained using the f_K scale [8] (see text).

and the logarithm of the cutoff are expected to be small for the physical values of the light quark masses. We calculated $\Delta_{l,s}$ on $N_\tau = 10$ lattices. Combining this with the published results of the HotQCD collaboration obtained on $N_\tau = 8$ and 12 lattices [8] we performed a continuum extrapolation. First we interpolated the lattice data for each N_τ using a smooth spline and estimated the error of the spline by bootstrap analysis. Next we performed a continuum extrapolation at selected values of temperature separated by 5 MeV within the interval $120 \text{ MeV} \leq T \leq 200 \text{ MeV}$ assuming a $1/N_\tau^2$ behavior. We studied the variation of the extrapolated result with varying the fit range in N_τ . These variations have been included in our final error estimate. For $T < 170 \text{ MeV}$ the $N_\tau = 6$ data have not been included in the analysis as they are incompatible with a $1/N_\tau^2$ behavior. For $T \leq 140 \text{ MeV}$ no $N_\tau = 12$ data are available so the extrapolation had to rely on $N_\tau = 8$ and $N_\tau = 10$ data only. The numerical results for different N_τ and as the continuum extrapolations are shown in Fig. 6. The continuum extrapolated results are slightly above the continuum results obtained with the stout action [14]. This difference is expected due to the slight difference in the light quark masses used in the two calculations, namely, $m_l = m_s/20$ versus $m_l = m_s/27$ in Ref. [14]. In Fig. 6 we also show the $N_\tau = 12$ HISQ data obtained using the lattice spacing determined from the kaon decay constant f_K [8]. These data are systematically above our continuum estimate.

Alternatively, we can get rid of the ultraviolet divergences in the quark condensate by considering the following combination, which is called the renormalized quark condensate [8]:

$$\Delta_q^R = d + 2m_s r_1^4 (\langle \bar{\psi}\psi \rangle_{q,\tau} - \langle \bar{\psi}\psi \rangle_{q,0}), \quad q = l, s. \quad (10)$$

Here d is a normalization constant that is related to the light quark condensate in the chiral limit. More precisely, $d = 2m_s r_1^4 \langle \bar{\psi}\psi \rangle_{l,0}(m_l \rightarrow 0)$. With the values of m_s and $\langle \bar{\psi}\psi \rangle_{l,0}(m_l \rightarrow 0)$ from Ref. [45] we get $d = 0.0232244$. The quantity defined in Eq. (10) is closely related to the renormalized quark condensate $\langle \bar{\psi}\psi \rangle_R$ introduced in Ref. [13]. Using our $N_\tau = 10$ results and the published HotQCD results for $N_\tau = 6, 8,$ and 12 we perform a continuum extrapolation for Δ_q^R . As for $\Delta_{l,s}$ we first perform a smooth spline interpolation and estimate the errors of the spline by bootstrap analysis. Then we perform a $1/N_\tau^2$ continuum extrapolation for selected values of the temperature separated by 5 MeV in the interval $120 \text{ MeV} \leq T \leq 200 \text{ MeV}$ based on the interpolation and its errors. We performed extrapolations using subsets of the available N_τ values and the differences in the obtained fit values for Δ_q^R were treated as systematic errors and entered into our final error estimate. For $T \leq 140 \text{ MeV}$ the continuum extrapolations are based on $N_\tau = 8$ and 10 data only.

The lattice QCD results for Δ_l^R and Δ_s^R are shown in Fig. 7, along with the continuum extrapolations. We also show the HISQ $N_\tau = 8$ data obtained using the lattice spacing from f_K in this figure which seem to agree quite well with our continuum result, except for $T > 180 \text{ MeV}$, where they are systematically lower. Our continuum results for Δ_l^R are slightly larger than the continuum results obtained with the stout action [14]. This is again expected to be due to the difference in the light quark masses (see discussion in Ref. [8]). Finally we would like to note the large difference in the temperature dependence of Δ_l^R and Δ_s^R . The decrease of the renormalized strange quark condensate is much more gradual than that of the light one and Δ_s^R reaches half of its vacuum value only at $T \simeq 200 \text{ MeV}$.

Acknowledgments

This work was supported by the U.S. Department of Energy under Contract No. DE-AC02-98CH10886. The numerical simulations have been performed at NERSC and on BlueGene/L computers at the New York Center for Computational Sciences (NYCCS) at Brookhaven National Laboratory. The smooth spline interpolation and bootstrap analysis was performed using the R package. We thank S. Mukherjee for his help with the R package and F. Karsch for reading the manuscript and useful comments. We also thank E. Megias, E. Ruiz Arriola, and L.L. Salcedo for reading the first version of this paper and pointing out the normalization error in the hadron resonance gas expression for the renormalized Polyakov loop, which we subsequently corrected.

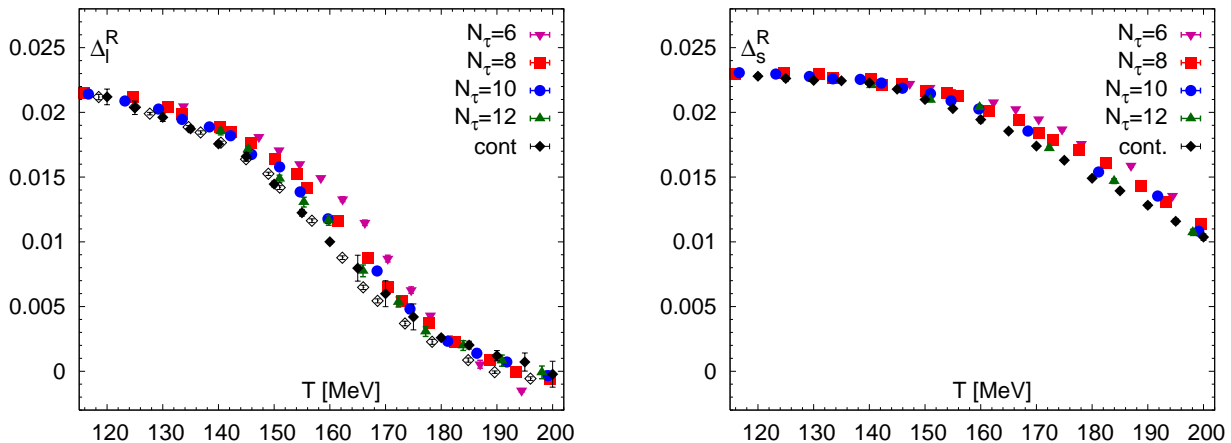


FIG. 7: The light (left) and strange (right) renormalized quark condensates calculated with the HISQ action. Open diamonds correspond to $N_\tau = 8$ HISQ results obtained with the f_K scale [8].

-
- [1] P. Petreczky, J.Phys. **G39**, 093002 (2012), 1203.5320.
[2] O. Philipsen, (2012), 1207.5999.
[3] O. Kaczmarek, F. Karsch, P. Petreczky, and F. Zantow, Phys. Lett. **B543**, 41 (2002), hep-lat/0207002.
[4] S. Digal, S. Fortunato, and P. Petreczky, Phys. Rev. **D68**, 034008 (2003), hep-lat/0304017.
[5] L. D. McLerran and B. Svetitsky, Phys. Rev. **D24**, 450 (1981).
[6] J. Kuti, J. Polonyi, and K. Szlachanyi, Phys. Lett. **B98**, 199 (1981).
[7] A. Bazavov *et al.*, Phys. Rev. **D80**, 014504 (2009), 0903.4379.
[8] A. Bazavov *et al.*, Phys. Rev. **D85**, 054503 (2012), 1111.1710.
[9] P. Petreczky, Eur. Phys. J. **C43**, 51 (2005), hep-lat/0502008.
[10] S. Digal, P. Petreczky, and H. Satz, Phys.Lett. **B514**, 57 (2001), hep-ph/0105234.
[11] Y. Aoki, Z. Fodor, S. Katz, and K. Szabo, Phys. Lett. **B643**, 46 (2006), hep-lat/0609068.
[12] M. Cheng *et al.*, Phys. Rev. **D77**, 014511 (2008), 0710.0354.
[13] Y. Aoki *et al.*, JHEP **0906**, 088 (2009), 0903.4155.
[14] Wuppertal-Budapest Collaboration, S. Borsanyi *et al.*, JHEP **1009**, 073 (2010), 1005.3508.
[15] HPQCD Collaboration, UKQCD Collaboration, E. Follana *et al.*, Phys. Rev. **D75**, 054502 (2007), hep-lat/0610092.
[16] E. Megias, E. Ruiz Arriola, and L. Salcedo, Phys.Rev.Lett. **109**, 151601 (2012), 1204.2424.
[17] E. Ruiz Arriola, E. Megias, and L. Salcedo, (2012), 1207.4875.
[18] E. Megias, E. Ruiz Arriola, and L. Salcedo, (2012), 1207.7287.
[19] ETM Collaboration, C. Michael, A. Shindler, and M. Wagner, JHEP **1008**, 009 (2010), 1004.4235.
[20] ETM Collaboration, M. Wagner and C. Wiese, JHEP **1107**, 016 (2011), 1104.4921.
[21] M. Clark, A. Kennedy, and Z. Sroczynski, Nucl. Phys. Proc. Suppl. **140**, 835 (2005), hep-lat/0409133.
[22] MILC collaboration, A. Bazavov *et al.*, Phys. Rev. **D82**, 074501 (2010), 1004.0342.
[23] MILC Collaboration, A. Bazavov *et al.*, PoS **LATTICE2010**, 074 (2010), 1012.0868.
[24] Y. Hatta and K. Fukushima, (2003), hep-ph/0311267.
[25] S. Digal, E. Laermann, and H. Satz, Eur.Phys.J. **C18**, 583 (2001), hep-ph/0007175.
[26] A. Mocsy, F. Sannino, and K. Tuominen, Phys.Rev.Lett. **92**, 182302 (2004), hep-ph/0308135.
[27] O. Jahn and O. Philipsen, Phys. Rev. **D70**, 074504 (2004), hep-lat/0407042.
[28] P. Huovinen and P. Petreczky, Nucl. Phys. **A837**, 26 (2010), 0912.2541.
[29] S. Borsanyi *et al.*, JHEP **1201**, 138 (2012), 1112.4416.
[30] HotQCD Collaboration, A. Bazavov *et al.*, (2012), 1203.0784.
[31] Particle Data Group, J. Beringer *et al.*, Phys.Rev. **D86**, 010001 (2012).
[32] G. Bali *et al.*, PoS **LATTICE2011**, 135 (2011), 1108.6147.
[33] S. Godfrey and N. Isgur, Phys.Rev. **D32**, 189 (1985).
[34] S. Godfrey and R. Kokoski, Phys.Rev. **D43**, 1679 (1991).
[35] D. Ebert, V. Galkin, and R. Faustov, Phys.Rev. **D57**, 5663 (1998), hep-ph/9712318.
[36] D. Ebert, R. N. Faustov, and V. O. Galkin, PoS **QCD-TNT-II**, 016 (2011).
[37] European Twisted Mass Collaboration, C. Alexandrou *et al.*, Phys.Rev. **D78**, 014509 (2008), 0803.3190.
[38] ETM Collaboration, R. Baron *et al.*, JHEP **1008**, 097 (2010), 0911.5061.
[39] S. Capstick and N. Isgur, Phys.Rev. **D34**, 2809 (1986).
[40] D. Ebert, R. Faustov, and V. Galkin, Phys.Rev. **D84**, 014025 (2011), 1105.0583.
[41] L. Y. Glozman, C. Lang, and M. Schrock, Phys.Rev. **D86**, 014507 (2012), 1205.4887.
[42] N. Brambilla, J. Ghiglieri, A. Vairo, and P. Petreczky,

Phys. Rev. **D78**, 014017 (2008), 0804.0993.

[43] A. Bazavov and P. Petreczky, (2012), 1210.6314.

[44] A. Bazavov and P. Petreczky, (2012), 1211.5638.

[45] A. Bazavov *et al.*, Rev. Mod. Phys. **82**, 1349 (2010), 0903.3598.